Stereo-Vision Based Free Space and Obstacle Detection with Structural and Traversability Analysis Using Probabilistic Volume Polar Grid Map

Jungwon Kang and Myung Jin Chung

Abstract— **The detection of free space and obstacles in a scene is essential for safe driving. Among sensors for environment perception, a stereo-vision is promising as it provides 3D perception information. Moreover current decreasing price of a camera module makes a vision sensor attractive, taking into account the consumer product. In this paper we propose an algorithm for the detection of free space and obstacles in a scene, using a stereo-vision. Contrary to previous generic obstacle detection methods that have a strong assumption of camera placement with respect to the ground or estimate ground parameters for free space/obstacles separation, our method analyzes 3D reconstructued structures of an environment. The environment is represented on the proposed probabilistic volume polar grid map. The probabilistic volume polar grid map is a simplified representation of the environment, using the volumes generated from the reconstructed point hypotheses. The volume polar grid map combines with an image plane, so that the reconstruction uncertainty representation and the free space computation are straightforward. The map is analyzed by the two ways: (1) the analysis of the structural characteristics of volumes and (2) the traversability analysis. The traversability analysis gives the free space and the nearest obstacle in each search direction, while the structural characteristics analysis provides potential obstacles in a more wide range. The results from both analysis modules are combined to provide information of the free space, obstacles and potential obstacles in the given scene, which is useful for safe driving. Our system is expected to be used as a driving assistance system.**

I. INTRODUCTION

The perception of free space and obstacles in a scene is essential for safe driving. Among various sensors [1] for scene perception, a stereo-vision is promising as it provides 3D perception data. Recent progress of processing techniques such as GPU [2] and FPGA [3] enables stereo reconstruction to run in real-time. Moreover current inexpensive camera module with high performance makes a vision sensor attractive, taking account of the consumer product.

Numerous vision based works have tried to detect a specific object that is important in a traffic scene. The object includes pedestrian [4], vehicle [5], bicycle [6] and so on. Their key interest is to select a discriminative feature and to design a classifier such as AdaBoost and SVM that classifies properly between features from a target object and non-target objects. In the case of the pedestrian detection, the feature can be a histogram of image gradient orientation [7] or a shape [8] in monocular vision case, a 3D point distribution [9] in stereo-vision case. Some stereo-vision based works have utilized a disparity image [10] and 3D data [11][12][13] for ROI(Region Of Interest) generation. However these kinds of specific object detection methods do not work properly when a target object is occluded by another objects or structures. Selection of proper scale for a detection window is also a difficult problem.

Meanwhile there have been stereo-vision based approaches for generic obstacle detection. They have focused on the binary classification problem of ground/obstacle separation. The methods are mainly categorized into three types: disparity map based, image remapping and 3D analysis method. First, the disparity map based methods [14][15] utilize a disparity histogram to estimate ground parameters, assuming that disparity pixels from the ground are dominant in the disparity image. Second, the image remapping method utilizes an image transformation for ground/obstacle separation [16][17][18]. One common technique is called the IPM(Inverse Perspective Mapping) [18]. The IPM is a transformation between the ground plane and the image plane. By the IPM two virtual ground images are generated from original stereo images. With the flat ground plane assumption, any difference in the two ground images represents non-ground objects, i.e. obstacles. A similar principle is also applied to the work in [19], that a stereo matching with the original and the ground-compliant matching windows is used instead of the image transformation. The methods mentioned above do not need the full 3D reconstruction. However they have several limitations. Real urban areas often do not have lane marking, and roads are occluded by crowded traffic. Such a scene makes it difficult to use the disparity histogram based method. The IPM method is sensitive to the error of the camera geometry with respect to the ground plane. Furthermore the planar ground assumption is often violated in a real environment. In order to overcome the limitations mentioned above, some works have analyzed a 3D model of an environment. In [20], obstacles are detected by checking connectivity of points in the reconstructed point cloud. To reduce computational load and complexity of 3D analysis, the use of simplified models such as an elevation map [21][22][23] is popular. In [23], the authors build an elevation map from reconstructed points and classify each elevation grid into road, traffic isle and an obstacle.

Jungwon Kang is a Ph.D. candidate in the Department of Electrical Engineering, Korea Advanced Institute of Science and Technology, 291 Daehak-ro, Yuseong-gu, Daejeon 305-701, Republic of Korea kctown@rr.kaist.ac.kr

Myung Jin Chung is a professor in the Department of Electrical Engineering, Korea Advanced Institute of Science and Technology, 291 Daehak-ro, Yuseong-gu, Daejeon 305-701, Republic of Korea mjchung@ee.kaist.ac.kr

In this paper we propose an algorithm for the detection of free space and generic obstacles in a scene, focusing on the analysis of a 3D environment model. The probabilistic volume polar grid map is proposed to represent an environment in a simplified probabilistic form. The elements in the volume polar grid map are evaluated by the structural characteristics and the traversability, providing the free space and obstacles in a scene.

This paper begins with an overview of the proposed algorithm in the upcoming section. In section III we describe the proposed probabilistic volume polar grid map. The detection of the free space and obstacles from the volume polar grid map is presented in section IV. We show experimental results in section V, and conclude this work in section VI.

II. Algorithm Overview

Our algorithm detects free space and generic obstacles by the analysis of a 3D environment model. The overview of our algorithm is shown in Fig. 1. In the first step, 3D points are reconstructed from given stereo image pairs. In order to model reconstruction uncertainty, we propose a probabilistic reconstruction method that represents a point as point hypotheses instead of an explicit point instance. The point hypotheses are generated, taking account of the depth uncertainty. The next step is to build a 3D model of an environment. The proposed probabilistic volume polar grid map represents the environment using volumes generated from the point hypotheses. The volume polar grid map is designed to combine with an image plane, so as to deal with the stereo uncertainty representation and the free space computation. The two-stage filtering process refines the map by eliminating insignificant components in the map.

The free space and obstacles are detected by the analysis of the volumes. The analysis consists of two parts: 1) the traversability analysis and 2) the structural characteristics analysis. This strategy is to find a free space defined as a traversable space from current vehicle position and to identify potentially dangerous structures. The traversability analysis includes the detection of the traversable volumes and the nearest obstacle in each search direction. The structural characteristics analysis identifies potential obstacles by calculating the obstacle likelihood based on the position, size, and point density of a volume. The results from both analysis modules are combined to provide information of the free space, obstacles and potential obstacles in a scene.

III. Probabilistic Volume Polar Grid Map

Taking into consideration the stereo uncertainty representation and the free space computation, we choose the polar grid space that combines with an image plane. The polar grid space is a suitable representation for modeling reconstruction uncertainty of the stereo-vision and computing the free space as every column of the grid is in the direction of a ray [24].

A. 3D Point Reconstruction By Stereo Triangulation

Assuming that the stereo cameras are calibrated and the stereo images are rectified, the reconstruction starts from

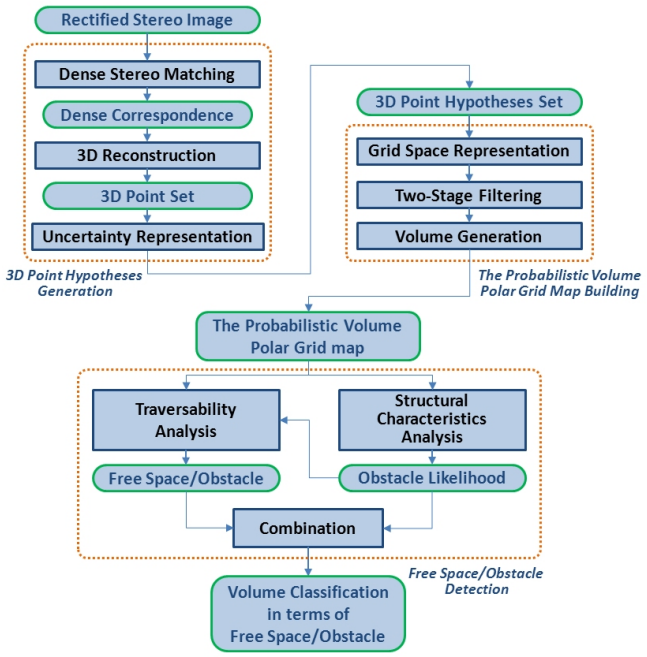

Fig. 1. An overview of our algorithm

calculating disparity associated to each pixel in the left image. The disparity d, the difference between corresponding pixels in the left and right images, is obtained by stereo matching algorithm.

For each measurement (x, y, d), the position (X_p, Y_p, Z_p) of a point in 3D space is calculated by (1), letting $\bar{x} = x - c_x$, $\bar{y} = y - c_y$ where (x, y) is a coordinate of the left image pixel, (c_x, c_y) is the principal point of the left image, L_B is the length of baseline and f is the focal length.

$$\begin{bmatrix} X_p \\ Y_p \\ Z_p \end{bmatrix} = R(x, y, d) = \frac{L_B}{d} \begin{bmatrix} \bar{x} \\ \bar{y} \\ f \end{bmatrix} \tag{1}$$

B. Depth-Adaptive Probabilistic Point Hypothesis Generation

Due to the image quantization, that is, dealing with 1 pixel reconstruction, the reconstruction by (1) has uncertainty over the position of a point. In order to deal with this reconstruction uncertainty, we represent a point as point hypotheses instead of an explicit point instance.

Suppose the measurement (x, y, d) is modeled as a normal distribution with covariance matrix $C_m = diag(\sigma_x^2, \sigma_y^2, \sigma_d^2)$ Then, with a first-order approximation of the triangulation equation, the position of a point in 3D space is represented as a normal distribution with covariance matrix $C_M = J_R C_m J_R^T$ where J_R is the Jacobian of R, given below.

$$C_M = \frac{Z_p^2}{L_B^2 f^2} \begin{bmatrix} L_B^2\sigma_x^2 + X_p^2\sigma_d^2 & X_pY_p\sigma_d^2 & X_pZ_p\sigma_d^2 \\ X_pY_p\sigma_d^2 & L_B^2\sigma_y^2 + Y_p^2\sigma_d^2 & Y_pZ_p\sigma_d^2 \\ X_pZ_p\sigma_d^2 & Y_pZ_p\sigma_d^2 & Z_p^2\sigma_d^2 \end{bmatrix} \tag{2}$$

We formulate the reconstruction problem as the problem of finding depth of each left image pixel. Therefore, for point hypothesis generation, we consider the depth uncertainty

given as a standard deviation $\sigma_Z = (Z_p^2\sigma_d)/(L_B f)$. In order to represent point hypotheses, we use a 3D grid space whose lateral and height components correspond to the image column and row respectively and depth axis is discretized with an interval Δ_Z, as shown in Fig. 2. The point density that is a probability of point existence is assigned to each cell within the depth uncertainty boundary. For the simplification of the depth uncertainty computation, we use a uniform distribution that is approximated from the normal distribution. The uncertainty of the uniform distribution is given by $\sigma'_Z = \eta\sigma_Z$ where η is a scaling parameter for approximation. Let L_u be the total length of uncertainty in the depth direction given by $L_u = 2\sigma'_Z$, L_c be the length that belongs to the uncertainty section for a cell, meaning the length in density voting range, $0 \leq L_c \leq \min(\Delta_Z, L_u)$. Then, the density L_c/L_u is voted to each cell such that $Z_p - \sigma'_Z \leq Z \leq Z_p + \sigma'_Z$.

C. Probabilistic Volume Polar Grid Map Building

The volume polar grid map is a 2D grid array where each cell in the grid stores a list of volumes that are hexahedron structure models. The map is similar to the multi-level surface map [25] and multi-volume occupancy grid map [26]. However, contrary to the other maps, the volume polar grid map is designed, combining with an image plane, to deal with reconstruction uncertainty and free space computation.

The volume polar grid map is described in Fig. 2. The predefined column interval Δ_L in pixels and the depth interval Δ_D determine the size and location of the cell in the lateral and the depth direction, respectively. Using the column interval Δ_L greater than one pixel enables a compact representation as in [27]. The depth interval Δ_D is defined as $c \cdot \Delta_Z$ where c is a predefined natural number. Let (i, j) be a cell index for the lateral and the depth direction respectively. Then the i corresponds to the image column x such that $\Delta_L \cdot i \leq x < \Delta_L \cdot (i+1)$ and the j corresponds to the depth Z such that $\Delta_D \cdot j \leq Z < \Delta_D \cdot (j+1)$.

In each cell, a volume is generated from the point hypotheses located within the cell area. In order to filter out insignificant hypotheses, we adopt two stage filtering process. The first stage eliminates hypothesis such that $\rho_h < \rho_{h,\min}(Z)$ where ρ_h is a point density of the hypothesis and $\rho_{h,\min}(Z)$ is a predefined minimum density that varies with the depth Z. Then the hypotheses within the height difference λ_g are considered to belong to the same group. In our case, $\lambda_g = 0.1m$. The second stage removes hypotheses group such that $\rho_g < \alpha N_p \rho_{h,\min}(Z)$ where ρ_g is the density summation of hypotheses in the group, α is a real positive constant and N_p is the number of image pixels that assign density to the group.

After the filtering process, the hypotheses are re-grouped so that the hypotheses within the height difference λ_v belong to the same group, represented by a volume. Here λ_v is the height that guarantees passing of the vehicle. In our case, $\lambda_v = 2.0m$, the height of the vehicle. Each volume is characterized by the properties: 3D position, height size S_v and point density ρ_v. The cell on the grid array determines

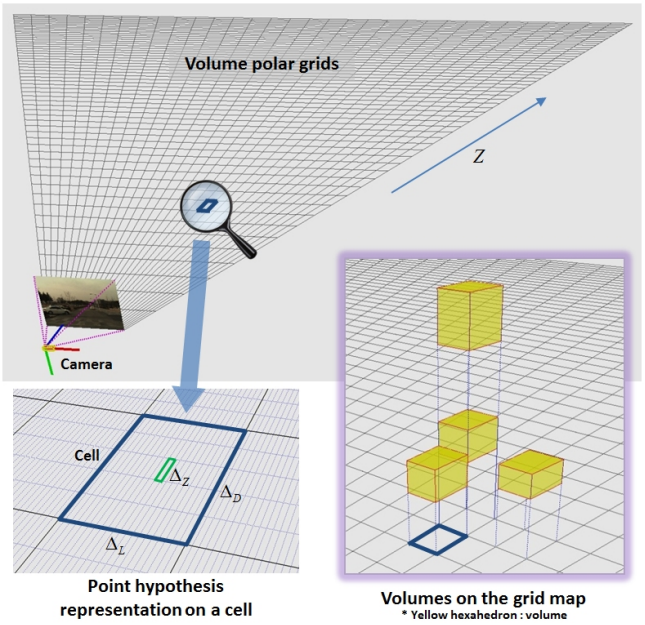

Fig. 2. The probabilistic volume polar grid map

the lateral(X) and the depth(Z) components of vertices of a hexahedron for the volume, while the height(Y) components of the vertices are set by the minimum and maximum Y values of the point hypotheses, defining the position and height size of the volume. The point density ρ_v of the volume is defined as $\rho_v = \sum_{i=1}^{N_h} \rho_h^i$ where N_h is the total number of hypotheses in the volume and ρ_h^i is the density of ith hypothesis.

IV. Free Space and Obstacle Detection

The volume polar grid map is analyzed, providing free space and obstacles in the map. Our initiative is to find a space that is traversable from the current vehicle position, and to identify structures to that the attention is needed for safe navigation.

The traversability analysis provides traversable volumes and the nearest non-traversable volume in each search direction. Here we let the free space be a space where navigation without collision is guaranteed. The free space is obtained by finding traversable volumes in each search direction. On the other hand, the obstacle is defined as the nearest volume that is not traversable in each search direction. Moreover, in order to identify volumes that could be dangerous in navigation, the likelihood of being an obstacle of each volume in the map is calculated based on the volume properties such as location, size and point density.

A. Structural Characteristics Analysis

The obstacle likelihood of each volume is evaluated based on the location, height size and point density of the volume. The traversability analysis that will be explained in the subsequent section provides only the nearest obstacle in each search direction, in terms of the obstacle detection.

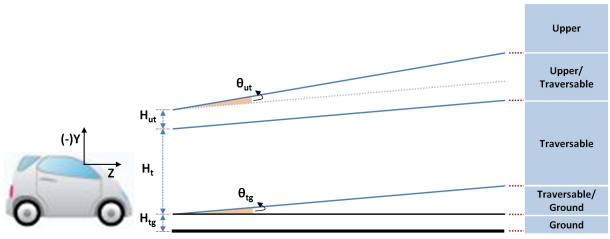

Fig. 3. The definition of areas

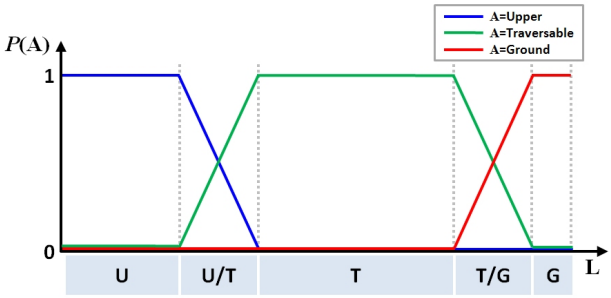

Fig. 4. The graph of $P(\mathrm{A})$

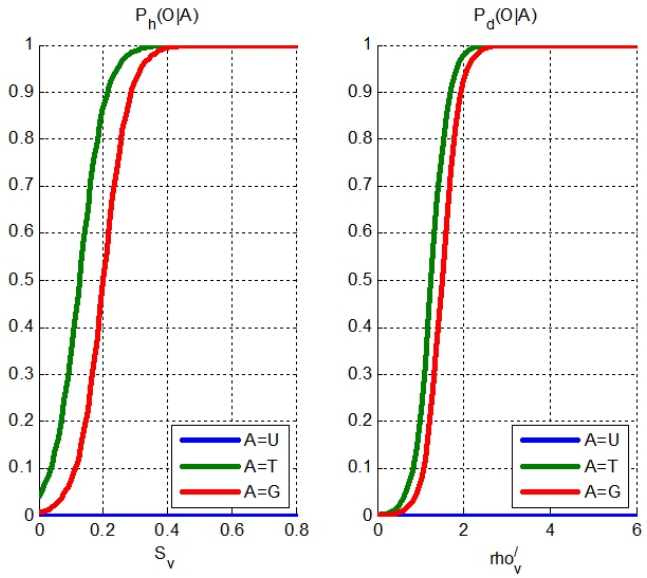

Fig. 5. The graph of $P_h(\mathrm{O|A})$ and $P_d(\mathrm{O|A})$

TABLE I
THE FORMULAS OF $P_h(\mathrm{O|A})$ AND $P_d(\mathrm{O|A})$

	$P_h(\mathrm{O\|A})$	$P_d(\mathrm{O\|A})$
A = U	0	0
A = T	$\frac{1}{1+e^{-\beta_{h,\mathrm{T}}(S_v - S_{0,\mathrm{T}})}}$	$\frac{1}{1+e^{-\beta_{d,\mathrm{T}}(\rho'_v - \rho'_{0,\mathrm{T}})}}$
A = G	$\frac{1}{1+e^{-\beta_{h,\mathrm{G}}(S_v - S_{0,\mathrm{G}})}}$	$\frac{1}{1+e^{-\beta_{d,\mathrm{G}}(\rho'_v - \rho'_{0,\mathrm{G}})}}$

On the other hand, as the evaluation in here is based on the structural characteristics of a volume regardless of traversability, the evaluation detects a more wide range of the obstacle candidates.

The insight of the potential obstacle detection is that a volume in the vehicle passing area and a volume with vertical shape on the ground are likely to be obstacles. Its likelihood as an obstacle increases with the height size and density of the volume. The calculation of the obstacle likelihood $P_s(\mathrm{O})$ of a volume consists of the computation of $P(\mathrm{A})$, the probability of an area A where a volume is located and $P_s(\mathrm{O|A})$, the probability of the volume being an obstacle at the area A, as in (3).

$$P_s(\mathrm{O}) = \sum_{\mathrm{A}=\{\mathrm{U,T,G}\}} P_s(\mathrm{O|A})P(\mathrm{A}) \tag{3}$$

Depending on the height of the vehicle with respect to the ground, we divide a space into the three areas: upper, traversable, ground, denoted as U, T, G, respectively, shown in Fig. 3. In addition, two transition areas (U/T), (T/G) are considered to model the uncertainty of the area boundary. In our case, we set $\mathrm{H_{tg}} = 0.1m$, $\theta_{tg} = 3.0°$, $\mathrm{H_t} = 2.0m$, $\mathrm{H_{ut}} = 0.2m$, $\theta_{ut} = 1.0°$. The $P(\mathrm{A})$ is calculated by the location L of a volume in the height direction, as in Fig. 4. The closest part of a volume to the area T in the height direction determines the location L of the volume. The $P_s(\mathrm{O|A})$ is the combination of the obstacle likelihood terms of the height size and the density of the volume. If the height size term $P_h(\mathrm{O|A}) > 0.99$ or the density term $P_d(\mathrm{O|A}) > 0.99$, $P_s(\mathrm{O|A}) = 1$. Otherwise, the $P_s(\mathrm{O|A})$ is calculated as in (4) where $w_h + w_d = 1$.

$$P_s(\mathrm{O|A}) = w_h P_h(\mathrm{O|A}) + w_d P_d(\mathrm{O|A}) \tag{4}$$

The $P_h(\mathrm{O|A})$ and the $P_d(\mathrm{O|A})$ are summarized in Table. I. The $P_h(\mathrm{O|A})$ evaluates a volume by the height size S_v of the volume. The $P_d(\mathrm{O|A})$ evaluates a volume by the density ratio ρ'_v of the volume, where $\rho'_v = \rho_v/\rho_{v,0}$, ρ_v is the density of the volume, $\rho_{v,0}$ is the criterion density that varies with the depth. The zero likelihood values are assigned to the volumes in the area U as the volumes are supposed not to interrupt the vehicle movement. Both $P_h(\mathrm{O|A})$ and $P_d(\mathrm{O|A})$ for the area T and G are designed to be logistic functions that show saturation as the height size and the density increase. The functions are characterized by the curve shape parameters and the shift parameters. The curve shape and the shift parameters are $(\beta_{h,\mathrm{T}}, S_{0,\mathrm{T}})$ for $P_h(\mathrm{O|A})|_{\mathrm{A=T}}$, $(\beta_{h,\mathrm{G}}, S_{0,\mathrm{G}})$ for $P_h(\mathrm{O|A})|_{\mathrm{A=G}}$, $(\beta_{d,\mathrm{T}}, \rho'_{0,\mathrm{T}})$ for $P_d(\mathrm{O|A})|_{\mathrm{A=T}}$ and $(\beta_{d,\mathrm{G}}, \rho'_{0,\mathrm{G}})$ for $P_d(\mathrm{O|A})|_{\mathrm{A=G}}$. The curve shape parameters are adjusted to have suitable transition of the likelihood values. The shift parameters are set to be $S_{0,\mathrm{T}} > S_{0,\mathrm{G}}$ for $P_h(\mathrm{O|A})$ and $\rho'_{0,\mathrm{T}} > \rho'_{0,\mathrm{G}}$ for $P_d(\mathrm{O|A})$ so that a volume in the area T has more likelihood than volumes in the area G. In our case, we set $(\beta_{h,\mathrm{T}}, S_{0,\mathrm{T}}) = (25.0m^{-1}, 0.125m)$, $(\beta_{h,\mathrm{G}}, S_{0,\mathrm{G}}) = (25.0m^{-1}, 0.2m)$, $(\beta_{d,\mathrm{T}}, \rho'_{0,\mathrm{T}}) = (5.0, 1.25)$, $(\beta_{d,\mathrm{G}}, \rho'_{0,\mathrm{G}}) = (5.0, 1.5)$ making the functions shown in Fig. 5.

B. Traversability Analysis

The traversability analysis includes the detection of the free space and obstacles, measuring the height difference of the upper planes of adjacent volumes and combining the

height difference-based evaluation with the structural obstacle likelihood $P_s(\mathrm{O})$. Finding the free space and obstacles is straightforward by means of the polar grid map. As every grid column is the direction of a ray leaving the camera, the search is performed along the depth direction, with the volumes located at the column. Note that the traversability analysis here performs a check on the volumes along the depth direction, without considering the vehicle width. The free space computation with the vehicle width can be easily obtained by the computation of the configuration space of the free space obtained here.

For the volumes with the cell column index i, the absolute difference of the maximum height of two consecutive volumes is checked, starting from the lowest row index $j = 0$, to determine the traversability between the two volumes. Here we only consider the lowest volume in the cell, as the lowest volume is considered to affect the traversability while the non-lowest volume is likely to be a structure at a high place. If a cell is empty, the maximum height of the preceding cell with a volume is propagated to the empty cell. Let $H_i(j)$ denote the maximum height in the (-)Y direction of a volume with cell index (i, j), $H_i(-1)$ be the height of the ground below the vehicle given as a prior information, T_r be a predefined traversable height difference such that $T_r > 0$. In our case, $T_r = 0.12m$, the vehicle wheel radius. The $P_t(\mathrm{O})$, the obstacle likelihood in terms of only the height difference-based traversability, is given as $\min(1.0, \Delta H_i(j-1, j)/T_r)$ where $\Delta H_i(j-1, j) = |H_i(j-1) - H_i(j)|$. Then the $P_t(\mathrm{O})$ combines with the $P_s(\mathrm{O})$, producing $P(\mathrm{O})$, the obstacle likelihood in terms of the traversability. If $P_s(\mathrm{O}) > 0.99$ or $P_t(\mathrm{O}) > 0.99$, $P(\mathrm{O}) = 1$. Otherwise, the $P(\mathrm{O})$ is calculated as in (5) where $w_s + w_t = 1$.

$$P(\mathrm{O}) = w_s P_s(\mathrm{O}) + w_t P_t(\mathrm{O}) \tag{5}$$

If $P(\mathrm{O}) < 0.5$, it is considered traversable from the $j-1$ volume to the j volume, and the volume with index (i, j) is registered as the free space volume. Otherwise, the volume is set as the obstacle volume. This search along the depth direction continues until an obstacle volume is detected or the search reaches the maximum depth range.

The traversability evaluation based on only the height difference often fails due to the sensing and the environment modeling error. The combination of $P_t(\mathrm{O})$ and $P_s(\mathrm{O})$ overcomes the problem.

C. Combination of the Results

The output from the structural and the traversability analysis consists of the free space, obstacles and potential obstacles. The free space are traversable volumes from the current vehicle position. The obstacles are the nearest non-traversable volumes in each search direction. The structures, located behind the obstacles, that could be dangerous by their structural characteristics are considered potential obstacles.

Fig. 6. The vehicle (left) with a stereo camera (right) on the top

V. Experimental Results

A. Experimental Setup

Our stereo camera is comprised of two CMOS cameras with 0.5m baseline. Each camera has a lens with 43.36° horizontal field of view. The stereo camera provides synchronized rectified images with size 640 $\times$ 480 in pixels at 30Hz. For the experiment, we have used only 640 $\times$ 290 pixels image region not to consider the sky in images. The stereo camera was installed on the vehicle as shown in Fig. 6. The height of the camera on the ground was 1.85m.

We have tested several dense stereo matching algorithms including our fast block matching based method [2]. Among the algorithms, the method of [28] has showed the great performance in terms of the accuracy. The current implementation of the method [28] runs at 4 frames/s, which is not enough speed for real-time operation. However we decided to use the method [28] since we have focused on the reconstruction accuracy and the speed performance would be improved as the processing technique develops.

B. Results

We have used a volume polar grid map with the column interval $\Delta_L = 10$ pixels and the depth interval $\Delta_D = 0.1m$. The Δ_Z is set equal to Δ_D. The maximum sensing depth is set to $50.0m$.

Fig. 7 shows how our algorithm works in detail. Volumes are generated from the reconstructed point hypotheses. By the structural characteristics analysis of the volumes, volumes with large height size or high density in the area T or G get high obstacle likelihood value, while flat volumes in the area G are considered non-obstacles. The common objects with high obstacle likelihood value are vertical objects such as pedestrians, cars, trees, and even the sidewalk border. The following traversability analysis finds traversable volumes and the nearest obstacle in each search direction of a ray. Due to the stereo reconstruction error and the environment model approximation by the volume polar grid map, the traversability evaluation using only the height difference of the volume upper planes often fails to detect the subtle structure like the sidewalk border. However our traversability evaluation, combined with the obstacle likelihood $P_s(\mathrm{O})$, has brought robustness to the sensing and modeling error. The final output includes the classification of the traversable volumes termed the free space, and the nearest non-traversable obstacle in each search direction, and the

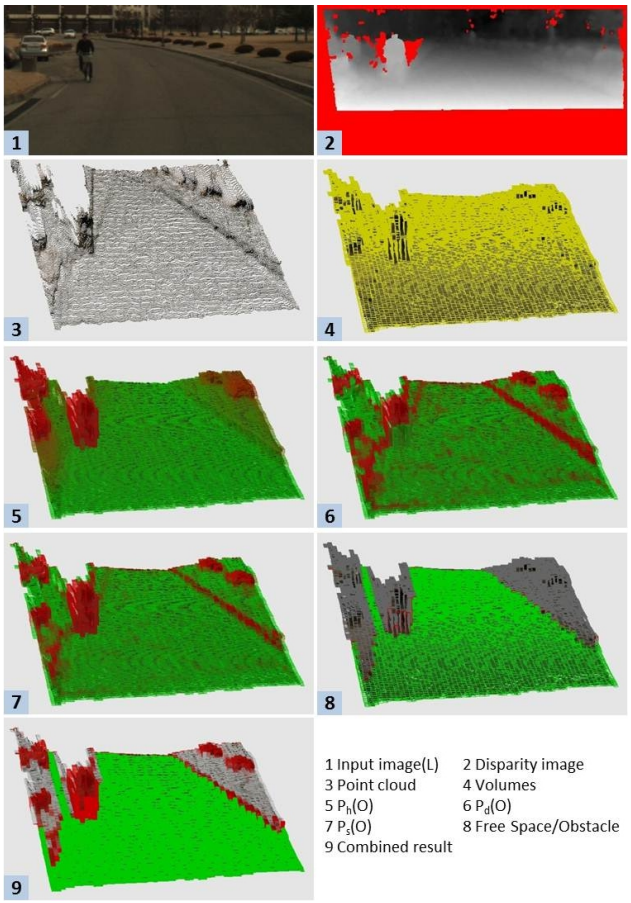

Fig. 7. Results showing the detection process. In the figures for $P_h(\mathrm{O})$, $P_d(\mathrm{O})$ and $P_d(\mathrm{O})$, the color varies from green to red as the obstacle likelihood increases. In the figure for the free space/obstacle detection result, a green volume is the free space, a red volume is an obstacle, and a gray one indicates a volume behind an obstacle. In the combined result, the color of a volume behind an obstacle changes from white to red as its obstacle likelihood increases.

potentially dangerous structures termed potential obstacles that are not the nearest in each search direction.

Fig. 8 shows a series of results for various scenes. The classification results are overlaid on the left input image. The green region indicates the free space, and the red region shows the obstacles such that $P(\mathrm{O}) \geq 0.5$ and the potential obstacles such that $P_s(\mathrm{O}) \geq 0.5$. Our method has successfully worked in the real scene. However our method is sensitive to the result of the dense stereo matching, as the suggested method is totally based on the 3D reconstruction data. Another limitation is related to the ground estimation. Our method uses the ground uncertainty model instead of definitely estimating the ground model parameters. Our ground uncertainty model, however, does not work when the real ground is largely out of the uncertainty region. The one example of the violation is the ground with steep slope.

C. Computation Time

On a PC with dual cores, it takes 65ms for the point hypotheses generation, 31ms for the volume generation, and almost zero for the structural characteristics and the traversability analysis. The total algorithm runs in 96ms, achieving more than 10 frames/s operation.

Considering many parts of the algorithm can be processed in parallel, the computation time could be significantly reduced if the algorithm is implemented using a parallel processing technique such as a GPU.

VI. Conclusion and Future Work

We have proposed a stereo-vision based free space and obstacle detection algorithm. The algorithm starts from building the probabilistic volume polar grid map. The proposed volume polar grid map combines with an image plane, so that the stereo uncertainty representation and the free space computation are straightforward. For the free space and obstacle detection, we have presented the combination of the potential obstacle detection based on the structural characteristics analysis and the traversability based free space computation. Comparing to the other methods that have a strong assumption of camera placement with respect to the ground or estimate the ground parameters, our algorithm focuses on the 3D structural analysis.

As a future work, we are going to work for the temporal integration of the multiple frame images, measuring the persistence of the map structure and providing the static and dynamic objects as well.

VII. ACKNOWLEDGMENTS

The authors gratefully acknowledge the support from UTRC(Unmanned technology Research Center) at KAIST (Korea Advanced Institute of Science and Technology), originally funded by DAPA, ADD.

References

[1] R. Sosa, G. Velazquez, "Obstacles detection and collision avoidance system developed with virtual models," *IEEE International Conference on Vehicular Electronics and Safety(ICVES)*, pp.1-8, 2007.

[2] S. U. Park, I. W. Shim, J. W. Kang, S. J. Kim, Y. G. Ryu, M. J. Chung, "Implementation of Dense Stereo Matching using GPU," *Workshop on Image Processing and Image Understanding*, Jeju, Korea, January, 2010.

[3] M. Devy, J.-L. Boizard, D. B. Galeano, H. C. Lindado, M. I. Manzano, Z. Irki, A. Naoulou, P. Lacroix, P. Fillatreau, J.-Y. Fourniols, C. Parra, "Stereovision Algorithm to be Executed at 100Hz on a FPGA-Based Architecture," *Advances in Theory and Applications of Stereo Vision*, 2011.

[4] D. Geronimo, A. M. Lopez, A.D. Sappa, T. Graf, "Survey of Pedestrian Detection for Advanced Driver Assistance Systems," *IEEE Transactions on Pattern Analysis and Machine Intelligence*, vol. 32 , issue 7, pp. 1239 - 1258, 2010.

[5] Zehang Sun, G. Bebis, R. Miller, "On-road vehicle detection: a review," *IEEE Transactions on Pattern Analysis and Machine Intelligence*, vol. 28, no. 5, pp. 694 - 711, May 2006.

[6] Hyunggi Cho, P.E. Rybski, Wende Zhang, "Vision-based bicycle detection and tracking using a deformable part model and an EKF algorithm," *2010 13th International IEEE Conference on Intelligent Transportation Systems (ITSC)*, pp. 1875 - 1880, 2010.

[7] N. Dalal and B. Triggs, "Histograms of oriented gradients for human detection," *In CVPR, Vol. 2, pp. 886-893*, June 2005.

[8] D. M. Gavrila and S. Munder, "Multi-cue Pedestrian Detection and Tracking from a Moving Vehicle," *International Journal of Computer Vision*, vol. 73, no. 1, pp. 41-59, June 2007.

[9] M. Bajracharya, B. Moghaddam, A. Howard, S. Brennan, L. H. Matthies, "A Fast Stereo-based System for Detecting and Tracking Pedestrians from a Moving Vehicle," *International Journal of Robotics Research*, vol. 28, issue 11-12, pp.1466-1485, 2009.

[10] H. Hattori et al, "Stereo-based Pedestrian Detection using Multiple Patterns," *In BMVC*, 2009.
[11] S. Nedevschi, S. Bota, and C. Tomiuc, "Stereo-Based Pedestrian Detection for Collision-Avoidance Applications," *IEEE Transactions on Intelligent Transportation Systems*, vol. 10, no. 3, pp. 380-391, September 2009.
[12] A. Toya et al, "Pedestrian Recognition using Stereo Vision and Histogram of Oriented Gradients," *IEEE International Conference on Vehicular Electronics and Safety(ICVES)*, pp. 57 - 62, 2008.
[13] M. Bansal, S.-H. Jung, B. Matei, J. Eledath and H. Sawhney, "A Real-time Pedestrian Detection System based on Structure and Appearance Classification," *2010 IEEE International Conference on Robotics and Automation*, May 2010.
[14] R. Labayrade, D. Aubert, J.P. Tarel, "Real time obstacle detection in stereovision on non flat road geometry through 'v-disparity' representation," *IEEE Intelligent Vehicle Symposium*, vol. 2, pp. 646-651, 2002.
[15] H. G. Jung, Y. H. Lee, B. J. Kim, P. J. Yoon, J. H. Kim, "Stereo Vision-based Forward Obstacle Detection," *International journal of Automotive Technology*, vol.8 no.4, pp. 493 - 504, 2007.
[16] S. Kubota, T. Nakano, Y. Okamoto, "A Global Optimization Algorithm for Real-Time On-Board Stereo Obstacle Detection Systems," *2007 IEEE Intelligent Vehicles Symposium*, pp. 7 - 12, 2007.
[17] Youchun Xu, Ming Zhao, Xiao Wang, Yongjin Zhang, Yongshen Peng, Yi Yuan, Hongquan Liu, "A method of stereo obstacle detection based on image symmetrical move," *2009 IEEE Intelligent Vehicles Symposium*, pp. 36 - 41, 2009.
[18] Ming Yang, Qian Yu, Hong Wang and Bo Zhang, "Vision-based real-time obstacle detection and tracking for autonomous vehicle guidance," *Proceedings Vol. 4666, Real-Time Imaging VI*, pp.65-74, February 2002.
[19] M. Perrollaz, A. Spalanzani, and D. Aubert, "A probabilistic representation of the uncertainty of stereo-vision and its application to obstacle detection," *IEEE Intelligent Vehicles Symposium (IV)*, pp. 313-318, June 2010.
[20] R. Manduchi, A. Castano, A. Talukder, and L. Matthies, "Obstacle detection and terrain classification for autonomous off-road navigation," *Autonomous Robots*, vol. 18, no. 1, pp. 81-102, 2005.
[21] M. Vergauwen, M. Pollefeys, and L. V. Gool, "A stereo-vision system for support of planetary surface exploration," *Machine Vision and Applications*, vol. 14, no. 1, pp. 5-14, April 2003.
[22] K. Kayama, I.E. Yairi, S. Igi, "Construction of elevation map for user-carried outdoor mobile robot using stereo vision," *IEEE International Conference on Systems, Man and Cybernetics*, pp. 4631 - 4636, 2003.
[23] F. Oniga, S. Nedevschi, "Processing Dense Stereo Data Using Elevation Maps: Road Surface, Traffic Isle, and Obstacle Detection," *IEEE Transactions on Vehicular Technology*, vol. 59, issue 3, pp. 1172 - 1182, March 2010.
[24] Hernan Badino, Uwe Franke and Rudolf Mester, "Free Space Computation Using Stochastic Occupancy Grids and Dynamic Programming," *Workshop on Dynamical Vision, ICCV*, Rio de Janeiro, Brazil, 20 October 2007.
[25] R. Triebel, P. Pfaff, W. Burgard, "Multi-Level Surface Maps for Outdoor Terrain Mapping and Loop Closing," *IEEE/RSJ International Conference on Intelligent Robots and Systems*, pp. 2276 - 2282, 2006.
[26] I. Dryanovski, W. Morris, J. Xiao, "Multi-volume occupancy grids: An efficient probabilistic 3D mapping model for micro aerial vehicles," 2010 IEEE/RSJ International Conference on Intelligent Robots and Systems (IROS), pp. 1553 - 1559, 2010.
[27] D. Pfeiffer, U. Franke, "Efficient representation of traffic scenes by means of dynamic stixels," *2010 IEEE Intelligent Vehicles Symposium (IV)*, pp. 217 - 224, 2010.
[28] Andreas Geiger and Martin Roser and Raquel Urtasun, "Efficient Large-Scale Stereo Matching," *Asian Conference on Computer Vision(ACCV)*, November 2010.

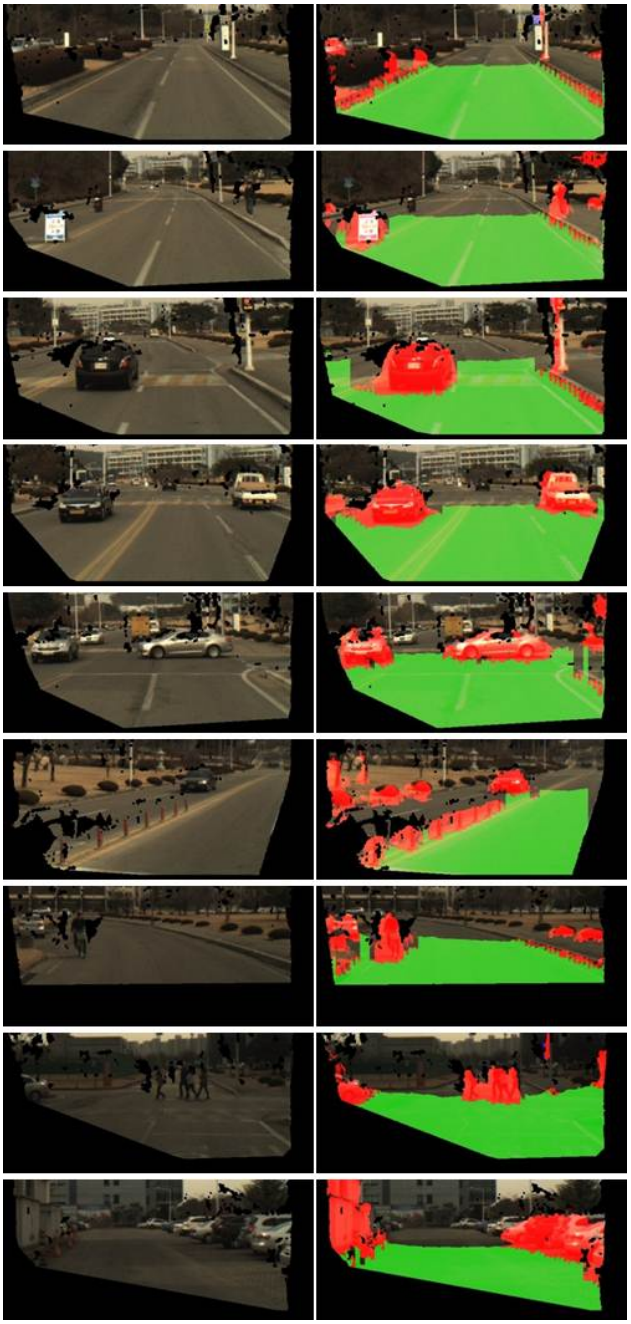

Fig. 8. Results for various scenes. Left input images (left) with only valid stereo matched region shown, and images overlaid with the detection result (right).